Comparison between Coreless and Yokeless Stator Designs in Fully-Superconducting Propulsion Motors

C. D. Manolopoulos, M. F. Iacchetti, *Senior Member, IEEE,* A. C. Smith, *Senior Member, IEEE,* P. M. Tuohy, X. Pei, P. Miller, and M. Husband

***Abstract*—Hybrid electric propulsion could be the solution to the ambitious environmental targets of the aerospace industry. Fully-superconducting machines have the potential to deliver the step-change in specific torque, power and efficiency capabilities required for large civil transport aircraft applications. However fully-superconducting machines are still in their infancy. This paper investigates the electromagnetic design of two different stator design concepts for an AC fully-superconducting machine for an aerospace distributed fan motor application. A benchmark aerospace specification of 1 MW was chosen and the design of a conventional permanent-magnet machine was used to assess the performance of the two equivalent fully-superconducting AC motor designs. Following the guidelines from an experimental study of the losses in a small AC stator prototype with MgB_2 coils, a fully-superconducting air-cored stator design and a new yokeless stator design are proposed. Both AC superconducting machine designs use superconducting bulk magnets mounted on a rotor core and an MgB_2 superconducting stator winding. This paper discusses the key design issues of the two stator layouts in relation to the current aerospace targets for efficiency and power density.**

***Index Terms*—AC superconducting losses, Aerospace hybrid-electric propulsion, Magnesium diboride, MgB_2 wire, Superconducting AC machine.**

I. Introduction

The aircraft industry has set ambitious emissions and noise reduction targets to meet the continual growth in global air traffic and the tightening environmental regulations [1], [2]. Meeting these targets has led to some radical proposals for future aerospace transportation technologies away from the traditional tube-and-wing concept. A promising novel concept is the use of hybrid electric distributed propulsion (HEDP) accompanied by a redesign of the airframe such as the hybrid wing body (HWB) [3]. Conventional electrical systems may be used for small aircraft applications with some projects in progress [4]. However for larger aircraft, superconducting electrical power systems may be required to achieve the increased power density and efficiency levels required [5]. The basic architecture of a HEDP system includes turboshaft engines driving electrical generators to supply a number of electric fan propulsion motors. The gas/generator units and the propulsion units are decoupled through the power management units, as studies have shown that this reduces the emissions and noise [6]. Superconducting machines could be the main component of this architecture, as they can potentially meet the stringent weight and loss constraints, enabling the hybrid electric aero-propulsion concept [7].

The first superconducting machines were large synchronous generators with superconducting DC field windings. The discovery of HTS allowed fully-superconducting machines to be considered. Fully-superconducting machines combine higher magnetic and electrical loadings. In addition, the operating temperature of the rotor windings and the stator armature are now similar, this facilitates a reduced air-gap compared to partially superconducting machines, further improving the magnetic loading. Prototypes of fully-superconducting machines have been developed worldwide. For example, a fully-superconducting motor for an electric vehicle and an inductor type fully-superconducting motor for ship propulsion were built in Japan [9], [10]. A synchronous motor with YBCO coils and YBCO bulks on the rotor was built in Cambridge, UK [11], and a superconducting stator with BSCCO coils cooled through the stator iron by conduction was developed in China [12]. Recently, fully-superconducting machines have been proposed for off-shore wind generators [13].

The operating frequency of motors for propulsion fans (up to a few hundred hertz) increase iron losses considerably and suggests minimizing or removing the stator iron core and relying on the superconducting rotor to maintain an adequate flux density. Despite the low mass and high power density achieved with a coreless stator, the AC superconducting windings are exposed to variable magnetic fields causing hysteretic losses in the superconductors,commonly called ‘magnetization losses’.

Manuscript receipt and acceptance dates will be inserted here. Acknowledgment of support is placed in this paragraph as well. This work was supported in part by the EPSRC, U.K., and in part by the Rolls-Royce plc.
(Corresponding author: C. D. Manolopoulos)

C. D. Manolopoulos was with the Power and Energy Division, School of Electrical and Electronic Engineering, The University of Manchester, Manchester M13 9PL, U.K. He is now with GKN Aerospace, Bristol BS37 7QQ, U.K. (email: charalampos.manolopoulos@gknaerospace.com).

M. F. Iacchetti, A. C. Smith, and P. M. Tuohy are with the Power and Energy Division, School of Electrical and Electronic Engineering, The University of Manchester, Manchester M13 9PL, U.K. (email: matteo.iacchetti@manchester.ac.uk; sandy.smith@manchester.ac.uk; paul.tuohy-2@manchester.ac.uk).

X. Pei is with Department of Electronic and Electrical Engineering, The University of Bath, Bath BA2 7AY, U.K. (email: x.pei@bath.ac.uk).

P. Miller and M. Husband are with the Rolls-Royce plc, Derby DE24 8BJ, U.K. (email: paul.miller3@rolls-royce.com; mark.husband@rolls-royce.com).

Color versions of one or more of the figures in this paper are available online at http://ieeexplore.ieee.org.

Digital Object Identifier will be inserted here upon acceptance.

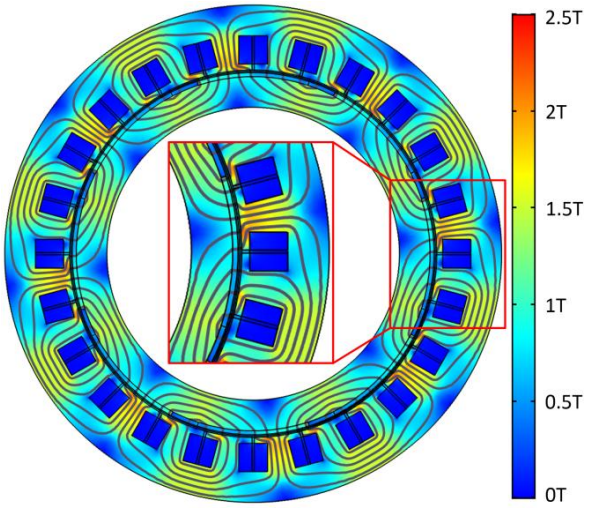

Fig. 1. FE model of the PM motor showing flux densities at full load.

Different methods have been developed to reduce the magnetic field seen by the superconductors including flux diverters [14], [15] but none of them seems to be satisfactory.

This paper presents a comparison between an air-cored and yokeless superconducting stator layout, which reduces the amount of iron whilst preserving a good shielding of the AC superconducting stator coils. This paper follows the preliminary work in [16] and includes experimental characterization of core and coil magnetization losses in a small prototype with a blank rotor to inform the design choices. A suitable benchmark aerospace specification is chosen and the design of a conventional PM machine is detailed and used to assess the performance of the fully-superconducting motor designs. Comparison with the benchmark PM machine will serve to highlight and inform some of the critical design decisions for aerospace superconducting machines.

II. Benchmark Aerospace HEDP Motor Specification

The benchmark motor specification has been chosen for a distributed electric fan motor for a short-haul aircraft. Siemens have recently developed a high power density 250 kW, 2,500 rpm, PM propeller motor for a single-engine light aircraft [17]. The power density is 5 kW/kg, which is significantly higher than normal industrial motors. The benchmark system here has been selected for a larger regional aircraft carrying typically 50-100 passengers and would have a number of larger motor driven fans. These commonly have a gearbox so that a high-speed motor can be used to reduce weight and improve the power density.

An electric fan motor with an output power of 1 MW and a maximum speed of 12,000 rpm was chosen. The AC PM machine will be used as the conventional benchmark machine. Both the PM and superconducting machine designs will have eight poles. This number of poles is typical for a PM machine of this size and speed. It is also assumed that a maximum phase voltage of 800 V_{rms} is available. This voltage is currently high for an aerospace application because of the high altitude. Nevertheless, it was chosen to keep the current levels down. Electrical systems voltage levels for aerospace applications have been increased over the last number of years and there are ongoing studies currently looking at even higher voltage levels [18].

TABLE I
Stator losses and efficiency for three different lamination steels

Lamination Steel	M400-50	Somaloy700	0.125mm Si
Core back loss (W)	9597	8714	2137
Teeth loss (W)	4131	3763	923
Tooth-tips loss (W)	1711	1559	382
Total stator iron loss (W)	15409	14036	3442
Copper armature loss (W)	2822	2822	2822
Total stator loss (W)	18231	16858	6264
Stator Efficiency[1] (%)	98.18	98.31	99.37

Stator efficiency is defined as the motor efficiency neglecting all the losses except the stator armature and iron losses.
[1] The stator efficiency is calculated for 1 MW nominal output power.

III. PM Motor Design and Performance

The PM motor design considers a surface-mounted PM rotor and a converter supply with the current in phase with the back emf. The rated torque is 800 Nm at full power, so assuming a 50% torque overload, the peak torque capability of the machine is 1200 Nm. The rotor has high-strength Nd–Fe–B magnets with a remanent flux density of 1.25 T. The leading machine dimensions are determined assuming a magnetic loading of 0.9 T (peak air-gap magnetic flux density), an electrical loading of 40,000 A/m and a current density of 6 A/mm^2. These values are a trade-off to achieve high power density (5.2 kW/kg) without compromising efficiency. A more comprehensive description of the PM design is given in [16].

As the main focus of the paper is the comparison between different superconducting stator designs, the rotor-core losses and eddy-current losses in the rotor PMs and stator armature were neglected. Therefore, a static FE model (Fig. 1) was the preferred modelling choice to estimate stator core losses. The iron losses were estimated by taking the average flux density in the stator back-iron, teeth and tooth-tips and using loss values in W/kg at 800 Hz for different commercial alloys, to calculate the total stator iron losses. Three different stator steels were assessed for the benchmark PM machine: a conventional 4 W/kg, 0.5 mm silicon steel; a low-loss thin-gauge silicon steel (0.125 mm lamination); and a soft-magnetic composite (Somaloy 700). The stator iron losses and the estimated efficiency for the three different laminations are summarized in Table I. As expected, the low-loss thin gauge steel lamination produces the highest efficiency – 99.37%.

IV. Experimental Stator Core and AC Winding

An experimental stator core was built and an MgB_2 round-wire winding was developed and tested to show that a superconducting AC stator winding could operate at significantly

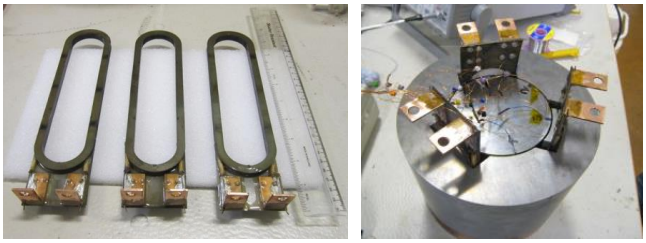

Fig. 2. MgB_2 stator coils (left) and small prototype test machine (right).

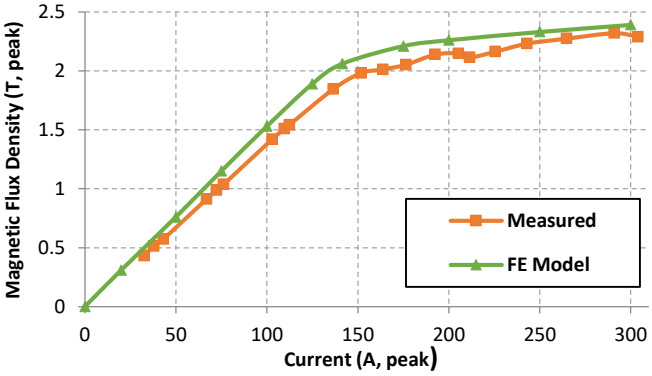

Fig. 3. Experimental and FE simulation air-gap flux density results.

higher AC magnetic field levels than those encountered in conventional electric machines, and also to evaluate the losses. The experimental stator was also used to assess the characteristics of cobalt-iron (CoFe) at cryogenic temperatures. A small prototype test machine was designed using CoFe laminations with a blank rotor and a simple 6-pole, three-coil, AC stator winding. The stator coils were designed to produce an air-gap magnetic flux density of 2 T compared to the typical air-gap field level of 0.9 T assumed in the PM benchmark machine. In order to maintain acceptable levels of tooth saturation, a tooth to coil width ratio higher than unity was adopted. That reduced the available space for the armature coils, but the higher operating current densities achievable in a superconductor maintained the electrical loading.

The stator coils were fabricated from 20 turns of Hyper Tech 0.83 mm MgB2 multi-core round wire, 70 micron size filaments with a Monel outer sheath, niobium barrier, copper matrix and S-glass insulation. It should be noted here that since the fabrication of these coils, Hyper Tech has developed several new types of low loss superconducting AC wires with orders of magnitude reduction in AC losses. The coils were wound onto high-resistance stainless steel formers, to facilitate a wind-react heat treatment, as shown in Fig. 2 (left). The stator magnetic core and the blank rotor were fabricated from Vacoflux 50 laminations. Six hall-effect magnetic sensors were mounted into the 1.5 mm air-gap, to measure the air-gap magnetic flux density. Fig. 2 (right) shows the full assembly of the stator and the rotor. The coils were energized with a single-phase power supply.

An FE model was built and was used to estimate that a 50 Hz AC coil current of approximately 140 A_{peak} would be required to establish a peak fundamental magnetic flux density of 2 T in the air-gap. The coils were tested at 50 Hz to avoid the copper stabilizer losses dominating and to focus predominately on the

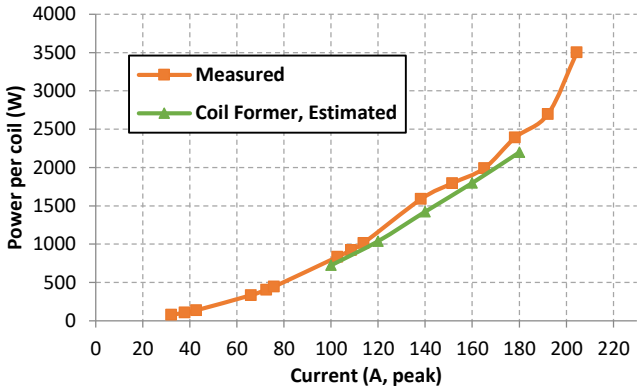

Fig. 4. Experimental and FE simulation power loss results.

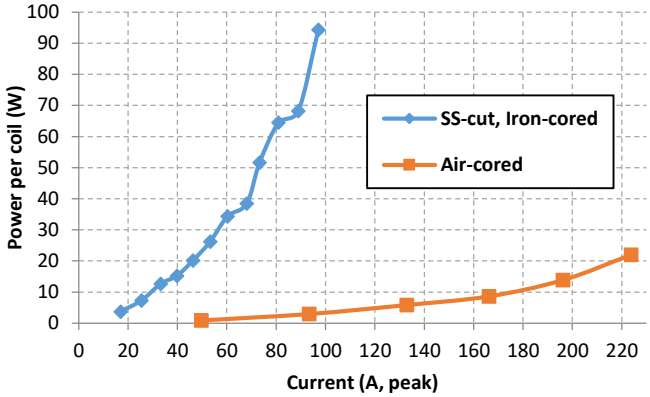

Fig. 5. Experimental losses with the stainless steel former cut for the iron-cored stator and losses of the original coils for an air-cored stator.

MgB_2 losses. The single-phase experimental tests were undertaken at 22 K and Fig. 3 illustrates the measured air-gap magnetic flux density results together with the FE model predictions. Fig. 3 demonstrates that an air-gap magnetic flux density of 2 T could be achieved successfully at a coil current of 156 A_{peak}, close to the estimated value of 140 A_{peak}. The results show that CoFe laminations have similar relative permeability at cryogenic and room temperatures. Finally, a maximum air-gap magnetic flux density level of 2.3 T was actually achieved but the required coil current increased significantly due to saturation of the CoFe core.

An electrical technique was used to measure the AC loss, described in [19]. The instantaneous current and voltage of the MgB_2 coils was used to produce the instantaneous power. The instantaneous power was then integrated over a cycle to obtain the real power P corresponding to the AC loss:

$$P = \int_0^T v_s \times i_s dt \tag{1}$$

where T is the period of the signal, v_s is the voltage across the MgB_2 coils and i_s is the current through the MgB_2 coils.

The loss measurements are illustrated in Fig. 4, and it is clear that there were significantly higher losses than expected for the coils and lamination steel. The estimated losses were expected to be approximately 100-200 W. The much higher measured losses were found to be caused by circulating eddy currents in

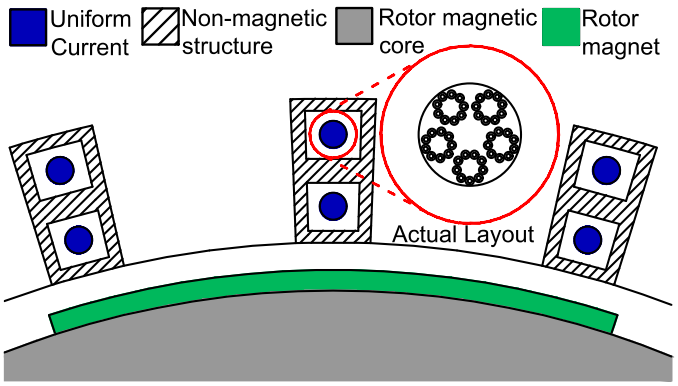

Fig. 6. Superconducting machine with air-cored stator. The boundary circle (red circle) is used to couple the machine model with the superconducting wire model.

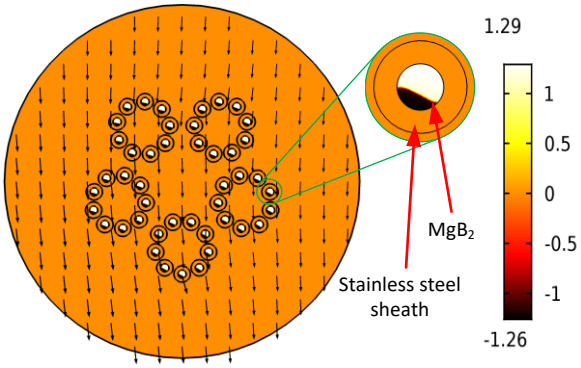

Fig. 7. Normalized current density distribution *J/Jc* in an inner-layer coil of the air-core stator after half an electrical period (south magnet below the slot). The coil has five turns composed of nine strands. Each strand carries the same current, as transposition is assumed. The close-up shows eddy currents in a single mono-core MgB2 wire that are causing the major losses. Although the total current is positive (white area), part of the wire has negative current (dark area). The sheath does not carry current.

the stainless steel coil formers used to heat treat the MgB_2 coils. Fig. 4 includes the estimated eddy current losses in the stainless steel coil former.

The stainless steel coil former from one of the coils was subsequently machined to remove a small section to open-circuit the former and that coil was re-tested. Fig. 5 confirms that the measured losses up to 100 A_{peak} were significantly reduced and were comparable with the estimated electrical steel core losses from the FE simulations. The MgB_2 losses were negligibly small in comparison to the electrical steel core losses at 50 Hz. The electrical steel stator core was subsequently removed and the coils were re-tested in an air-core effectively. Fig. 5 shows clearly the reduction in total losses by removing the electrical steel stator core. The measured average losses at 150 A_{peak} were approximately 7 W per coil but this included the stainless steel coil former losses, and losses in the cryostat containment (estimated at 1.55 W [19]) so the measured AC losses in the MgB_2 wire for each coil were approximately 5.45 W.

The conclusion from the experimental tests on the AC stator winding using MgB_2 coils and a CoFe core was that the coils could operate in a machine with a high air-gap magnetic field close to 2 T. Initially the majority of the losses were found to occur in the stainless steel coil former, so it is important to ensure the coil formers are ideally non-conducting. The losses were found to reduce significantly when one of the coil formers was open-circuited. Even with an open-circuited former, the high losses of the iron lead to a thermal quench after several supply cycles. Mass savings aside, this is another reason that the stator iron of a superconducting machine should be either totally removed or minimized. An alternative would be to operate the iron at high (non-cryogenic) temperature.

V. Superconducting AC Machine

A. Air-cored Stator Design

Following the conclusions from the experimental results in Section IV, a superconducting machine design with an air-cored stator was initially chosen. Similarly to the PM machine design, the superconducting equivalent will have a maximum speed of 12,000 rpm and 800 V_{rms} terminal voltage. The same electric loading of the benchmark PM motor design (40 kA/m) was adopted to allow direct comparison. The rotor was assumed to have superconducting coils in place of the PM blocks. The rotor core design itself was not modified; it simply mirrored the PM rotor design. The high magnetic fields produced by the superconducting coils were created by changing the remanent flux density of the blocks. Further work in optimizing the rotor design would be expected to provide additional benefits in terms of electric machine weight savings. The main aim of this study, however, was directed at the requirements of a superconducting stator. The stator core was chosen initially to be non-magnetic, to reduce the weight and eliminate the iron losses. The stator winding was the same as the conventional PM machine design described in Section III but using round MgB_2 wire. Fig. 6 shows part of the stator and rotor FE model; the double-layer stator coils are mounted in non-magnetic formers and placed as close to the machine air-gap as possible to minimize the reduction in the operating air-gap magnetic field due to the non-magnetic stator core.

Hyper Tech 0.36 mm mono-core round wire was used to model the armature windings. This wire was designed for superconducting fault current limiters so it has a high resistive steel sheath around the MgB_2 core. This mono-core wire had previously demonstrated satisfactory low-loss and consistent performance. Due to the air-cored stator, the maximum magnetic field seen by the superconductors is 1.37 T. The estimated peak current density for this maximum magnetic field, assuming a 20 K operating temperature, was 1.5 kA/mm^2. The stator has 24 slots and to achieve the rated back-emf, the stator winding has five turns per stator coil, with two coils in series and four groups in parallel. The current of each coil is 140 A_{rms}, so nine strands were used in each coil, as seen in the actual layout of Fig. 6. Given the 25% fill factor of the MgB_2 wire, each strand is operating at approximately 58% of the critical current. This would allow up to approximately 50% machine overload. The magnetic loading for the superconducting machine was chosen to be slightly higher compared to the benchmark PM machine design, to compensate for the high field decay through the stator and the consequent flux linkage reduction. The first

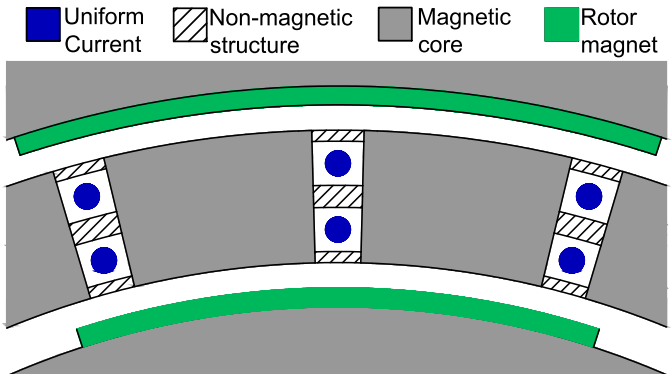

Fig. 8. Superconducting machine with yokeless stator design.

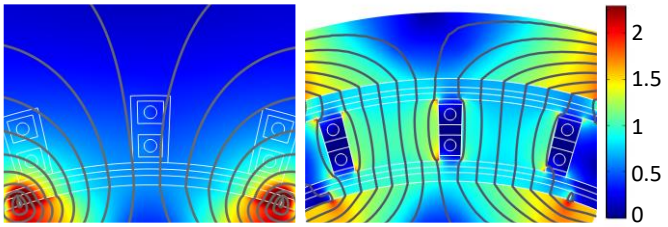

Fig. 9. Magnetic field distribution for air-cored (left) and yokeless (right) AC superconducting machine stator design. The field seen by the conductors is considerably lower for the yokeless stator design.

harmonic of the magnetic field at the air-gap, therefore, was 1 T for the superconducting machine; compared to the benchmark PM machine, which had a peak air-gap field of 0.9 T.

To estimate the superconducting losses in the armature, the machine FE model was coupled indirectly with the superconducting wire FE model. The machine FE model neglects the superconducting properties of the wire, and a uniform current density is applied to obtain the magnetic field distribution of the machine. The tangential component of the magnetic field around the boundary circle (red circle in Fig. 6) from the machine FE model is applied to the wire FE model, shown in Fig 7, as a boundary condition [20]. The wire FE model calculates the current distribution in each superconducting strand and finally the superconducting losses. The superconducting wire FE model uses the H-formulation to obtain the current distribution using the real arrangement of the conductors.

The governing equation used in the wire FE model is:

$$\nabla \times \left(\rho \nabla \times \mathbf{H}\right) + \frac{\partial \left(\mu \mathbf{H}\right)}{\partial t} = 0 \qquad (2)$$

where ρ is the resistivity (Ωm); μ is the permeability (H/m); and, H is the magnetic field strength (A/m). The sheath of the MgB_2 wire has a constant resistivity of 540 nΩm. The non-linear resistivity of the MgB_2 wire is modelled using the power law: $\rho_{sc}=(E_0/J_c)(J/J_c)^{n-1}$ where the voltage criterion, E_0, is 1 μV/cm and the power law index, n, is 30. Although the critical current density varies with temperature and magnetic field at the superconductor, we used a constant J_c value to avoid excessive calculation time. Fig. 7 shows the superconducting wire FE model and the current distribution for an inner-layer coil. The major loss factor for an air-cored stator is the magnetization loss at the superconductors because of their exposure to the main rotor magnetic field.

TABLE II
SUPERCONDUCTING MOTORS DIMENSIONS

Dimensions in (mm)	Air-cored Stator	Yokeless Stator
Axial length	300	300
Shaft radius	124	124
Inner rotor iron mean radius	137	137
Inner rotor iron thickness	26	26
Inner Airgap radius	155.7	155.7
Stator iron mean radius	-	170
Stator iron thickness	-	24
Outer airgap radius	-	184.4
Outer rotor iron mean radius	-	203
Outer rotor iron thickness	-	26
Outer radius	190	216

B. *Yokeless Stator Design*

The high magnetization losses at the superconductors are the main issue of the air-cored stator design in Section V. As previous attempts to minimize the superconductor exposure to magnetic fields using diverters were unsatisfactory [14], [15], here, an alternative yokeless stator design is proposed and analyzed. This configuration tries to combine low magnetic field seen by the conductors and minimum use of stator iron following the guidelines from the experimental results. Fig. 8 shows part of the machine FE model; in this configuration, the stator yoke has been removed and an external rotor has been placed to guide the flux. The floating teeth in the stator provide a low reluctance path for the flux between the two air-gaps and screen the stator coils. The big difference is the magnetic field seen by the superconducting wire between the two designs, which is shown in Fig. 9. The dimensions of the two superconducting designs are given in Table II.

To assess the benefits of the different superconducting machine designs, the magnetic and electric loadings were kept the same as in the air-cored stator design (40 kA/m and 1 T, respectively). CoFe electrical steel (Vacoflux 50) was used for the stator segments because it has a high saturation flux density. The rotor iron losses were again neglected, as in the PM benchmark machine. The stator teeth iron losses were calculated using the magnetic field of each element of the mesh for one electrical cycle. The manufacturer's material loss data were then interpolated to calculate the losses in each element for the flux density and rated frequency (800 Hz). The total iron loss in the yokeless stator was estimated by adding the loss in each element. It is also assumed that the stator iron operates at high temperature. This would typically cause high temperature gradients across the insulation of the coils but it was chosen in this design to reduce the load at the cryo-coolers. Finally, the superconducting armature losses were calculated using the same procedure as in the air-cored superconducting design described in the previous section.

TABLE III
ESTIMATED STATOR EFFICIENCY AND POWER DENSITY FOR DIFFERENT MACHINE DESIGNS

Design Parameter	Conventional PM motor (0.125 Si)	Superconducting AC motor	
		Air-cored Stator	Yokeless Stator
Output power (kW)	1000	850.7	1249
Mean torque (Nm)	800	677	994
St. iron loss (W)	3442	0	3314
St. armature loss (W)	2822	5378	304
St. cold 'inefficiency'[1] (%)	-	0.63	0.024
St. efficiency (%)	99.37	99.37	99.71
St. weight (kg)	134.6	14.7	49
Rotor weight (kg)	57	58	144
Power density[2] (kW/kg)	5.2	11.7	6.5

The electrical loading is the same for all the designs. The magnetic loading is 0.9 T for the PM motor and 1 T for the superconducting motors.

[1]This is defined as the armature superconducting losses in the cryogenic system as a percentage of the machine output power [21].

[2]The power density does not include mechanical support structures.

VI. RESULTS

Table III compares the performance of the superconducting designs against the benchmark PM motor design. The power density of the air-cored stator superconducting machine has been significantly improved compared to the conventional PM motor. The analysis here focused only on the electromagnetic design, a full design study including the mechanical and cooling details would give further insight into the mass figures. As a result, the mass shown in Table III is only the active weight and does not include frame, shaft, cooling, etc. One of the issues in an air-cored design is the conductors have to support the full developed torque. It was assumed here that the MgB_2 coils were mounted into an annular cylinder fabricated from fiberglass-fiber-reinforced composite, which avoids eddy current losses and can achieve strength/weight ratios higher than titanium [22]. The annular composite stator could also include cooling channels if necessary for the cryogen, depending on the cooling design chosen. As a result, the estimated weight of the composite is considered as active and it is included in the total stator mass presented in Table III for the air-cored design.

The air-cored stator superconducting motor design has a similar efficiency with the benchmark PM motor design. However, the superconducting coils operate at 20 K and would require a large cryo-cooling system. A feasibility study undertaken for an HEDP system suggests a machine 'cold inefficiency' lower than 0.05% is needed [21]. The air-cored stator design, although very light, would be unlikely to achieve this target. The proposed yokeless superconducting stator motor design, however, has manageable superconducting losses because the segmented teeth reduce the magnetic field seen by the superconducting coils but the added external rotor doubles the rotor weight. This extra weight keeps the power density similar to the power density of the conventional PM motor design.

It should be noted here that the iron teeth improve the magnetic performance of the stator, so less powerful superconducting magnets are required compared to the air-cored stator design. This would possibly enable additional benefits in terms of rotor weight. Nevertheless, at this stage the rotor design was kept the same for all the machine designs and only the remanent flux density of the rotor magnets was changed. Besides the added weight, another potential problem with the external rotor of the yokeless stator superconducting motor design would be the mechanical integrity of the structure at high speed (12,000 rpm), particularly the stator. However, this issue could be alleviated by changing the topology to an axial flux design [23].

VII. CONCLUSION

This paper investigated the feasibility of two different stator designs (air-cored and yokeless) of a fully-superconducting motor for an aerospace distributed fan motor application. A benchmark motor specification of a conventional PM motor design based on an electric fan motor for a short-haul aircraft was used as a comparator. The high-level design of the PM machine showed that it would be difficult to achieve motor efficiencies greater than 99% without resorting to specialist magnetic stator core steels but it would still be unlikely to achieve the target efficiency figures in excess of 99.9% suggested in recent aerospace studies.

Experimental work using a cobalt-iron stator with MgB_2 coils showed that iron losses are the major loss factor and they should be removed or minimized. As a result, an air-cored stator design was chosen and assessed. This design has a significantly higher power density than the conventional PM motor design. However, due to the high losses at the stator conductors, this design has similar efficiency to the PM motor. The increased losses would also cause problems to the cryogenic cooling system. Partially-superconducting air-cored designs with litz wire at the armature have also been proposed to reduce the high armature losses [23].

A fully-superconducting yokeless stator design was proposed here to screen the conductors from the rotor magnetic field and at the same time minimize the iron used in the stator. The fully-superconducting machine design with the yokeless stator has a predicted efficiency close to the target of 99.9% and a power density equal to 6.5 kW/kg. The efficiency is significantly higher than that of the air-cored stator design and the power density is slightly better than that of the conventional PM motor design. It should be noted that these efficiency figures will be an over-estimation because they ignore harmonic, stray and mechanical losses. The key issue with this configuration would be the mechanical construction and integrity of the structure but this may be eased using an axial flux machine topology.

The analysis suggests that the proposed specifications are a breakpoint between conventional and superconducting machines. At higher torque or power ratings, superconductivity will offer improved benefits. This breakpoint could be reduced with methods to reduce the magnetization losses. Multifilament wires are commonly preferred for low AC losses, but careful attention is needed on the coupling losses and the additional eddy current losses in the copper stabilizer used in their manufacture. Superconducting materials with improved performance

in a magnetic field and winding techniques that reduce the magnetic field seen by the superconductors would enable fully-superconducting electric machines to outperform conventional electric machines at lower power and torque levels.

REFERENCES

[1] S. Kallas, *et al.*, "Flightpath 2050 Europe's Vision for Aviation," *Report of the High Level Group on Aviation Research, European Commission, Brussels, Belgium, Report No. EUR,* vol. 98, 2011.

[2] F. Collier and R. Wahls, "NASA ARMD Strategic Thrust 3: Ultra-Efficient Commercial Vehicles Subsonic Transport," presented at the Aeronautics R&T Roundtable, Washington DC, USA, 2016.

[3] J. L. Felder, G. V. Brown, H. DaeKim, and J. Chu, "Turboelectric distributed propulsion in a hybrid wing body aircraft," in *20th ISABE conference*, Gothenburg, Sweden, 2011.

[4] M. Caujolle and R. Gage. Airbus, Rolls-Royce, and Siemens team up for electric future Partnership launches E-Fan X hybrid-electric flight demonstrator. Available: http://www.airbus.com/newsroom/press-releases/en/2017/11/airbus--rolls-royce--and-siemens-team-up-for-electric-future-par.html (accessed: 30 January 2018)

[5] P. Malkin and M. Pagonis, "The design of fully superconducting power networks for future aircraft propulsion," in *49th AIAA/ASME/SAE/ASEE Joint Propulsion Conference*, San Jose, CA, 2013.

[6] F. Berg, J. Palmer, P. Miller, M. Husband, and G. Dodds, "HTS Electrical System for a Distributed Propulsion Aircraft," *IEEE Trans. Appl. Supercond.*, vol. 25, no. 3, Jun 2015, Art. no. 14907083.

[7] C. A. Luongo, *et al.*, "Next Generation More-Electric Aircraft: A Potential Application for HTS Superconductors," *IEEE Trans. Appl. Supercond.*, vol. 19, no. 3, pp. 1055-1068, Jun 2009.

[8] S. S. Kalsi, *et al.*, "Development status of rotating machines employing superconducting field windings," in *Proceedings of the IEEE*, 2004, pp. 1688-1704.

[9] D. Sekiguchi, *et al.*, "Trial Test of Fully HTS Induction/Synchronous Machine for Next Generation Electric Vehicle," *IEEE Trans. Appl. Supercond.*, vol. 22, no. 3, Jun 2012, Art. no. 5200904.

[10] T. Takeda, H. Togawa, and T. Oota, "Development of liquid nitrogen-cooled full superconducting motor," *IHI Eng. Rev.*, vol. 39, no. 2, p. 89, 2006.

[11] Z. Huang, M. Zhang, W. Wang, and T. A. Coombs, "Trial Test of a Bulk-Type Fully HTS Synchronous Motor," *IEEE Trans. Appl. Supercond.*, vol. 24, no. 3, Jun 2014, Art. no. 4602605.

[12] T. M. Qu, *et al.*, "Development and testing of a 2.5 kW synchronous generator with a high temperature superconducting stator and permanent magnet rotor," *Supercond. Sci. Technol.*, vol. 27, no. 4, Apr 2014.

[13] X. Song, N. Mijatovic, B. B. Jensen, and J. Holbøll, "Design Study of Fully Superconducting Wind Turbine Generators," *IEEE Trans. Appl. Supercond.*, vol. 25, no. 3, pp. 1-5, 2015, Art. no. 5203605.

[14] C. D. Manolopoulos, *et al.*, "Stator Design and Performance of Superconducting Motors for Aerospace Electric Propulsion Systems," *IEEE Trans. Appl. Supercond.*, vol. 28, no. 4, pp. 1-5, 2018, Art. no. 5207005.

[15] F. Gomory, M. Vojenciak, E. Pardo, and J. Souc, "Magnetic flux penetration and AC loss in a composite superconducting wire with ferromagnetic parts," *Supercond. Sci. Technol.*, vol. 22, no. 3, p. 034017, Mar 2009.

[16] C. D. Manolopoulos, *et al.*, "Design of Superconducting AC Propulsion Motors for Hybrid Electric Aerospace," in *2018 AIAA/IEEE Electric Aircraft Technologies Symposium*, Cincinnaty, Ohio, 2018.

[17] Siemens. Record-breaking motor is 'five times more powerful' *Drives and Controls Magazine*. Available: http://drivesncontrols.com/news/fullstory.php/aid/4758/Record-breaking_motor_is__91five_times_more_powerful_92.html (accessed: 7 January 2018)

[18] I. Cotton, R. Gardner, D. Schweickart, D. Grosean, and C. Severns, "Design considerations for higher electrical power system voltages in aerospace vehicles," in *2016 IEEE IPMHVC*, San Francisco, CA, 2016, pp. 57-61.

[19] X. Z. Pei, A. C. Smith, and M. Barnes, "AC Losses Measurement and Analysis for a 2G YBCO Coil in Metallic Containment Vessels," *IEEE Trans. Appl. Supercond.*, vol. 27, no. 4, Jun 2017, Art. no. 5900605.

[20] V. M. R. Zermeno, *et al.*, "Simulation of an HTS Synchronous Superconducting Generator," *Physics Procedia*, vol. 36, pp. 786-790, 2012.

[21] F. Berg, J. Palmer, P. Miller, and G. Dodds, "HTS System and Component Targets for a Distributed Aircraft Propulsion System," *IEEE Trans. Appl. Supercond.*, vol. 27, no. 4, Jun 2017, Art. no. 3600307.

[22] H. Sugimoto, *et al.*, "Development and test of an axial flux type PM synchronous motor with liquid nitrogen cooled HTS armature windings," *8th European Conference on Applied Superconductivity (Eucas'07)*, vol. 97, 2008.

[23] K. S. Haran, D. Loder, T. O. Deppen, and L. J. Zheng, "Actively Shielded High-Field Air-Core Superconducting Machines," *IEEE Trans. Appl. Supercond.*, vol. 26, no. 2, pp. 98-105, Mar 2016, Art. no. 5202508.